Supporting Information

Akat et al. 10.1073/pnas.1401724111

SI Materials and Methods

Tissue Procurement. Nonfailing (NF) postnatal cardiac tissue was obtained from the National Human Tissue Resource Center (National Disease Research Interchange, Philadelphia). Five fetal heart specimens (gestational age 19–24 wk) were obtained after elective termination of pregnancy for nonmedical reasons. Failing myocardial samples and blood for serum and EDTA-plasma preparation from patients with heart failure (HF) were obtained from the Columbia University Medical Center. Serum and EDTA–plasma samples of healthy controls were also obtained from the Columbia University Medical Center. The tissue samples were immediately flash frozen in liquid nitrogen upon harvesting and stored at −80 °C until processing. Informed consent was obtained from all human subjects, and the ethics committees of the participating institutions approved the study (Institutional Review Board Protocol KAK-0750–0611 from The Rockefeller University and Protocol IRBAAAE2296 from Columbia University).

Clinical and Demographic Data. Summarized patient characteristics and selected clinical data are available in Tables S1 and S2 (myocardial samples and serum and plasma samples, respectively), and individual level patient data are listed in Dataset S1 (Table 34). No invasive assessments of hemodynamics were performed during the 3 and 6 mo follow-up outpatient clinic visits of advanced HF patients in the serum–plasma cohort.

RNA Isolation. Total RNA from tissue and plasma samples was isolated with a modified TRIzol protocol and recovered by ethanol precipitation. Tissue samples were homogenized in 20× volume of TRIzol using a mechanical bead mill. After thawing, the plasma samples were centrifuged at 16,000 × *g* at 4 °C for 5 min to remove residual debris, and 500 μL were homogenized by vortexing with 3× volume of TRIzol LS. After the initial homogenization and isopropanol precipitation, myocardial tissue samples were additionally treated with DNase I [0.2 U/μL final concentration (f.c.)] for 30 min at 37 °C, and both myocardial and plasma samples were digested with proteinase K (100 μg/mL f.c. in a buffer containing 0.5% SDS) for 20 min at 42 °C before a second phenol chloroform extraction. The samples were precipitated twice in the presence of 0.3 M NaOAc (pH 5.2) with 3 volumes of 100% ethanol at −20 °C for at least 1 h, collected by centrifugation for 30 min at 16,000 × *g*, and resuspended in RNase-free water. All precipitation steps of the plasma samples were done in the presence of glycogen at a final concentration of 40 μg/mL as a carrier. The RNA composition may vary according to the used RNA isolation protocol, and RNA isolations using the TRIzol protocol as described by the manufacturer without carrier skews the microRNA (miRNA) distribution in low concentration RNA samples (1). However, using carrier glycogen, we did not observe any depletion of possibly affected miRNAs, e.g., miR-21. For the microarray studies, the RNA was additionally processed using Qiagen RNeasy columns as described in the manufacturer's manual.

The RNA concentration and purity was determined by microvolume UV spectrophotometry (NanoDrop; Thermo Scientific) or using the fluorometric Qubit RNA Assay (Molecular Probes; Life Technologies). The RNA integrity of the tissue RNA samples was determined by a microchip based capillary electrophoresis (Agilent Bioanalyzer 2100).

sRNA Library Preparation and Analysis. The cDNA library preparation for the tissue samples was done according to our published protocol (2). Briefly, total RNA was ligated to a 3′-oligonucleotide adapter containing a 5-nt barcode at the 5′-end allowing the pooling of up to 20 samples in one flow lane and at the same time preserving strand orientation and minimizing intersample variation. An equimolar mixture of 10 synthetic 22-nt calibrator oligoribonucleotides were spiked in at this step. These spike-in controls have no match in the human genome and served as quality control and quantification. The samples were pooled and size-selected by 15% denaturing polyacrylamide gel electrophoresis and gel eluted, followed by 5′-adapter ligation and another gel purification. The ligated RNA was reverse transcribed using SuperScript III reverse transcriptase (Life Technologies) and the RNA was hydrolyzed by alkaline hydrolysis. For the tissue libraries, the RNA input was 1–2 μg and the amount of spiked-in oligoribonucleotide mixture 0.25 fmol each per microgram of total RNA. The input for the serum or plasma samples was the total RNA from 0.5 mL starting material, and the oligoribonucleotide amount was reduced to 0.005 fmol for each calibrator per sample. One sRNA cDNA library for plasma and serum samples (library 8) was not spiked with calibrator oligonucleotides. In addition, the tissue libraries were also spiked-in with radiolabeled size markers that facilitated size selection (19 and 24 nt). These were digested with PmeI after PCR amplification; the serum and plasma samples did not contain size markers. The libraries were amplified by 7–12 cycles (tissue) or 12–16 cycles (plasma) of PCR, and loaded onto a 2.5% (wt/vol) agarose gel for gel purification using the Qiagen Gel extraction kit. The eluted cDNA was sequenced on an Illumina GAIIx or HiSeq 2000 sequencer in the Genomic Core Facility at The Rockefeller University.

Bioinformatics Analysis of RNA Sequencing. The FASTQ output files from the HiSeq 2000 were analyzed using a pipeline as described previously (3, 4). The files were demultiplexed, the 3′-adapters trimmed, and sequences between 16 and 35 nt aligned to the human genome build 37 allowing one mismatch, and allowing two mismatches to curated RNA transcriptomes for miRNAs as well as rRNAs, tRNAs, small cytoplasmic RNAs (scRNAs), small Cajal body-specific RNAs (scaRNAs), snRNAs, small nucleolar RNAs (snoRNAs), circular RNAs (circRNAs), and bacterial plasmid references used in recombinant protein expression (3, 4). The reads were aligned with the short read aligner Burrows-Wheeler Alignment tool (5). For the unsupervised clustering analysis, we restricted the set of miRNAs to the ones within the top 85% sequence reads in at least one sample, for which we can measure regulatory effects. The dataset included 10 technical replicates that clustered reproducibly. Unsupervised hierarchical clustering was performed using Euclidean distance and complete linkage for columns (samples) and rows (miRNAs or mRNAs) unless indicated otherwise; for the sake of clarity the row dendrograms were removed from the figures (with exception of Fig. S6). The differential expression (or levels in the case of plasma samples) analysis was done with the R/Bioconductor package edgeR (Version 3.3.5) (6–8). The reads were normalized using the weighted trimmed mean of *M* values (9) and normalized for library size. We kept only miRNAs with one read per million reads in at least five samples for the differential expression/levels analysis. The differences were tested using the exact test for unpaired samples, or by an additive generalized linear model (GLM) for paired samples with the patients as the blocking factor. The read variation was estimated

using tagwise or common dispersion for the exact test and the GLM, respectively. In the biological myocardial replicates this variation was typical for what has been reported in other RNA-sequencing (RNAseq) studies (the biological coefficient of variation was between 0.44 and 0.51) (10) and the variability in the plasma samples was higher (the biological coefficient of variation ranged from 0.59 to 0.84). Differences were considered significant below a false discovery rate (FDR) (11) of 10%.

Bioinformatics Analysis of mRNA Expression Arrays. The mRNA gene expression experiments of selected subsamples were performed on the HumanHT-12v4 bead arrays from Illumina. For the in vitro transcription and RNA labeling, 200 μg total RNA were used as input with the Ambion MessageAmp Premier RNA Amplification Kit (Life Technologies), and the amplified RNA (aRNA) quality checked by microfluidic analysis (Bioanalyzer 2100). For each sample, 750 ng aRNA was hybridized to a section of the Illumina BeadArrays. aRNA synthesis and hybridization were done by the Genomics Core Facility at The Rockefeller University. The arrays were scanned on a BeadScan station, and the analysis was based on the bead level data using R (Version 3.1) (12) and the Bioconductor 2.13 beadarray (2.12.0) (13–16), lumi (2.14.1) (17, 18), and limma (3.18.3) (19–21) packages. The arrays were transformed by variance-stabilizing transformation (18) followed by robust spline normalization probes with a match category "bad" or "no match" to the genome or transcriptome were removed after normalization (22), as were probes matching to the Y chromosome due to the uneven or unknown sex distribution. The moderated *t* statistic was used to test for differential expression (19). Reported expression differences are for an FDR of 10% [Benjamini and Hochberg (11)] unless stated otherwise.

Analysis of miRNA–mRNA Correlations. The functional studies testing miRNA regulation followed the approach by Grimson et al. (23). We only considered probes with intensity at least above the median, allowed only one miRNA target site per miRNA and transcript, and did not allow nested sites. We also tested the effects on highly expressed genes, defined as probe intensities above the 75th percentile. The 3′UTRs and the coding sequences were downloaded from Ensembl (Versions 67 and 71, respectively; www.ensembl.org), and in cases of multiple transcripts per gene the longest isoform was used.

Cardiac Troponin I and B-Type Natriuretic Peptide ELISAs. Cardiac troponin I (cTnI) and B-type natriuretic peptide (BNP) were both measured by a chemiluminescent microparticle immunoassay performed for quantitative determination of BNP in plasma or cTnI in serum using the ARCHITECT iSystem (Abbott).

Other Statistical Analyses. All statistical analyses were done in the R statistical language. Differences in RNA quantification for unpaired samples were tested using the Kruskal–Wallis rank sum test; for paired samples, the Wilcoxon signed rank test was used. The differences in the empirical cumulative distributions were tested using one-sided Kolmogorov–Smirnov. For all tests, an alpha level of 0.05 was considered significant. To compare the performance of circulating miRNAs and cTnI as biomarker, a two-class area under the curve was computed.

List of Tables in Dataset S1

Table 1. Differential expression analysis of miRNA cistrons comparing FET with NF in myocardium.
Table 2. Differential expression analysis of individual miRNAs comparing FET with NF in myocardium.
Table 3. Differential expression analysis of miRNA sequence families (sf) comparing FET with NF in myocardium.
Table 4. Differential expression analysis of miRNA cistrons comparing dilated cardiomyopathy (DCM) HF with NF in myocardium.
Table 5. Differential expression analysis of individual miRNAs comparing DCM HF with NF in myocardium.
Table 6. Differential expression analysis of miRNA families comparing DCM HF with NF in myocardium.
Table 7. Differential expression analysis of miRNA cistrons comparing DCM left ventricular assist device (LVAD) with DCM HF in myocardium.
Table 8. Differential expression analysis of individual miRNAs comparing DCM LVAD with DCM HF in myocardium.
Table 9. Differential expression analysis of miRNA families comparing DCM LVAD with DCM HF in myocardium.
Table 10. Differential expression analysis of miRNA cistrons comparing ischemic cardiomyopathy (ICM) HF with NF in myocardium.
Table 11. Differential expression analysis of individual miRNAs comparing ICM HF with NF in myocardium.
Table 12. Differential expression analysis of miRNA families comparing ICM HF with NF in myocardium.
Table 13. Differential expression analysis of miRNA cistrons comparing ICM LVAD with DCM HF in myocardium.
Table 14. Differential expression analysis of individual miRNAs comparing ICM LVAD with DCM HF in myocardium.
Table 15. Differential expression analysis of miRNA families comparing ICM LVAD with DCM HF in myocardium.
Table 16. Identified SNPs of miRNAs in all samples of non-failing postnatal, fetal, and failing myocardium. The nucleotide position of the detected variation in the stem–loop precursor, the type of base variation, the genomic coordinated, the SNP identifier in dbSNP 131, and the corresponding location in the precursor region are given.
Table 17. Differences in mRNA levels comparing each DCM HF, ICM HF, and FET with NF (reference). Only transcripts/probes with an adjusted *P* value [FDR, Benjamini and Hochberg (11)] <10% were included.
Table 18. Differences in mRNA levels comparing DCM/ICM LVAD with DCM/ICM HF, i.e., expression changes after LVAD support. Results are reported for DCM and ICM combined. Results are from paired samples, i.e., a sample from a different time point from the same patient. Only transcripts/probes with an adjusted *P* value [FDR, Benjamini and Hochberg (11)] <10% were included.
Table 19. Analysis of miRNA changes in plasma based on miRNA cistrons comparing advanced HF with NF.
Table 20. Analysis of miRNA changes in plasma based on individual miRNAs comparing advanced HF with NF.
Table 21. Analysis of miRNA changes in plasma based on miRNA families comparing advanced HF with NF.
Table 22. Analysis of miRNA changes in plasma based on miRNA cistrons comparing 3-mo LVAD samples with advanced HF samples.
Table 23. Analysis of miRNA changes in plasma based on individual miRNAs comparing 3-mo LVAD samples with advanced HF samples.
Table 24. Analysis of miRNA changes in plasma based on miRNA families comparing 3-mo LVAD samples with advanced HF samples.
Table 25. Analysis of miRNA changes in plasma based on miRNA cistrons comparing 6-mo LVAD samples with advanced HF samples.
Table 26. Analysis of miRNA changes in plasma based on individual miRNAs comparing 6-mo LVAD samples with advanced HF samples.

Table 27. Analysis of miRNA changes in plasma based on miRNA families comparing 6-mo LVAD samples with advanced HF samples.
Table 28. Analysis of miRNA changes in plasma based on miRNA cistrons comparing samples at LVAD explantation with NF.
Table 29. Analysis of miRNA changes in plasma based on individual miRNAs comparing samples at LVAD explantation with NF.
Table 30. Analysis of miRNA changes in plasma based on miRNA families comparing samples at LVAD explantation with NF.
Table 31. Analysis of miRNA changes in plasma based on miRNA cistrons comparing stable HF with NF.
Table 32. Analysis of miRNA changes in plasma based on individual miRNAs comparing stable HF with NF.
Table 33. Analysis of miRNA changes in plasma based on miRNA families comparing stable HF with NF.
Table 34. Individual-level demographics for all samples.
Table 35. Details on the sRNAseq samples.
Table 36. Details on the read annotation for all sRNAseq samples.
Table 37. ELISA levels for serum cTnI and plasma BNP.
Table 38. Curated miRNA reference used for the read annotation.
Table 39. Definitions of miRNA cistrons and sf.

Explanation of Annotation Categories in Dataset S1, Table 36

Adapter: 3′-Adapter sequences (Dataset S1).

Calibrator: Synthetic oligoribonucleotides spiked-in into samples (for sequences and details, see ref. 24). Note: No oligoribonucleotide cocktail was spiked-in into library 8 (serum and plasma library).

RecombProtein: Sequences related to the recombinant expression of enzymes needed for the library preparation.

SizeMarker: Synthetic oligoribonucleotides that are 19 and 24 nt (35 nt) and used for size fractionation during the sRNAseq library preparation. Note: spiked-in only in the solid tissue and cell line libraries, and PmeI digested before sequencing (for sequences and details, see ref. 11).

Genome: Sequences mapping to the human genome but to none of the RNA annotations.

Unmapped: Sequences not mapping to any of the annotation categories or to the human genome.

circRNA: Circular RNAs.

lincRNAs: Large intergenic noncoding RNAs.

mRNA: Messenger RNAs.

miRNA: MicroRNAs.

mt_Genome: Reads mapping to the mitochondrial chromosome.

mt_mRNA: Reads mapping to the mitochondrial mRNA transcriptome.

mt_tRNA: Reads mapping to mitochondrial tRNAs.

piRNA: Reads mapping to Piwi-interacting RNAs.

rRNA and rRNAPrec: Reads mapping to ribosomal RNAs and ribosomal RNA precursors.

scRNA and scRNAPrec: Small cytoplasmic RNAs and precursors. This includes Y RNAs RNY1, and RNY3-5, vault RNAs (vtRNAs) 1 and 2, and signal recognition particle (7SL) RNAs with editing variants.

scaRNA and scaRNAPrec: Small Cajal body-specific RNAs and precursors.

snRNA and snRNAPrec: Small nuclear RNAs and precursors.

snoRNAs and snoPrec: Small nucleolar RNAs and precursors.

tRNA and tRNAPrec: tRNAs and precursors.

1. Kim YK, Yeo J, Kim B, Ha M, Kim VN (2012) Short structured RNAs with low GC content are selectively lost during extraction from a small number of cells. *Mol Cell* 46(6):893–895.
2. Hafner M, et al. (2012) Barcoded cDNA library preparation for small RNA profiling by next-generation sequencing. *Methods* 58(2):164–170.
3. Farazi TA, et al. (2012) Bioinformatic analysis of barcoded cDNA libraries for small RNA profiling by next-generation sequencing. *Methods* 58(2):171–187.
4. Brown M, Suryawanshi H, Hafner M, Farazi TA, Tuschl T (2013) Mammalian miRNA curation through next-generation sequencing. *Front Genet* 4:145.
5. Li H, Durbin R (2009) Fast and accurate short read alignment with Burrows-Wheeler transform. *Bioinformatics* 25(14):1754–1760.
6. Robinson MD, McCarthy DJ, Smyth GK (2010) EdgeR: A bioconductor package for differential expression analysis of digital gene expression data. *Bioinformatics* 26(1):139–140.
7. Robinson MD, Smyth GK (2007) Moderated statistical tests for assessing differences in tag abundance. *Bioinformatics* 23(21):2881–2887.
8. Robinson MD, Smyth GK (2008) Small-sample estimation of negative binomial dispersion, with applications to SAGE data. *Biostatistics* 9(2):321–332.
9. Robinson MD, Oshlack A (2010) A scaling normalization method for differential expression analysis of RNA-seq data. *Genome Biol* 11(3):R25.
10. McCarthy DJ, Chen Y, Smyth GK (2012) Differential expression analysis of multifactor RNA-Seq experiments with respect to biological variation. *Nucleic Acids Res* 40(10):4288–4297.
11. Benjamini Y, Hochberg Y (1995) Controlling the false discovery rate: A practical and powerful approach to multiple testing. *Journal of the Royal Statistical Society Series B (Methodological)* 57(1):289–300.
12. R Core Team (2013) *R: A language and environment for statistical computing* (R Foundation for Statistical Computing, Vienna, Austria). Available at www.R-project.org. Accessed July 1, 2014.
13. Dunning MJ, Smith ML, Ritchie ME, Tavare S (2007) Beadarray: R classes and methods for Illumina bead-based data. *Bioinformatics* 23(16):2183–2184.
14. Dunning MJ, Barbosa-Morais NL, Lynch AG, Tavaré S, Ritchie ME (2008) Statistical issues in the analysis of Illumina data. *BMC bioinformatics* 9:85.
15. Cairns JM, Dunning MJ, Ritchie ME, Russell R, Lynch AG (2008) BASH: A tool for managing beadarray spatial artefacts. *Bioinformatics* 24:2921–2922.
16. Barbosa-Morais NL, et al. (2010) A re-annotation pipeline for Illumina beadarrays: Improving the interpretation of gene expression data. *Nucleic Acids Res* 38:e17.
17. Du P, Kibbe WA, Lin SM (2008) Lumi: A pipeline for processing Illumina microarray. *Bioinformatics* 24(13):1547–1548.
18. Lin SM, Du P, Huber W, Kibbe WA (2008) Model-based variance-stabilizing transformation for Illumina microarray data. *Nucleic Acids Res* 36(2):e11.
19. Smyth GK (2004) Linear models and empirical bayes methods for assessing differential expression in microarray experiments. *Stat Appl Genet Mol Biol* 3(1):Article3.
20. Smyth GK (2005) Bioinformatics and Computational Biology Solutions using R and Bioconductor, eds Gentleman R, Carey V, Dudoit S, Irizarry R, Huber W (Springer, New York), pp 397–420.
21. Ritchie ME, et al. (2006) Empirical array quality weights in the analysis of microarray data. *BMC Bioinformatics* 7:261.
22. Ritchie ME, Dunning MJ, Smith ML, Shi W, Lynch AG (2011) BeadArray expression analysis using bioconductor. *PLOS Comput Biol* 7(12):e1002276.
23. Grimson A, et al. (2007) MicroRNA targeting specificity in mammals: Determinants beyond seed pairing. *Mol Cell* 27(1):91–105.
24. Hafner M, et al. (2012) Barcoded cDNA library preparation for small RNA profiling by next-generation sequencing. *Methods* 58(2):164–170.

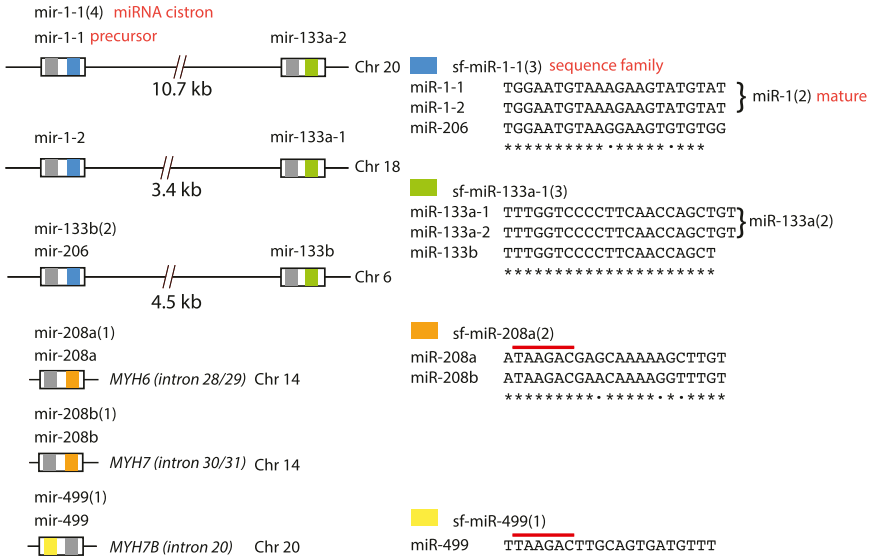

Fig. S1. Grouping of miRNA deep-sequencing reads based on the principles of genomic organization and sequence homology by myomir example. The outlined boxes show miRNA stem–loop precursors with colored rectangles representing guide strands color-coded for the different miRNA sequence family (sf); gray-shaded rectangles depict star strands. The miR-1-1(3) and miR-133a-1(3) family members are organized in two-member cistrons that are expressed under the control of their own promoters. The mir-208a/b(1) and mir-499(1) cistrons are located in the introns of the myosin genes *MYH6*, *MYH7*, and *MYH7B,* respectively, and are excised from the pre-mRNA. sRNAseq reads may be reported either by (*i*) matching mature sequences [e.g., miR-1(2)] with the number in parentheses indicating the number of genes encoding identical mature sequences, by (*ii*) reads matching miRNAs belonging to a cistron [e.g., mir-1-1(4)], the number in parentheses indicating mature sequences encoded in that cistron; or by (*iii*) reads matching miRNA sf members [e.g., sf-miR-1-1(3)], with the number in parentheses indicating mature reads with identical bases in positions 2–7 and at maximum 50% mismatch in the remaining sequence. Asterisks and dots indicate similarities and differences in the alignments, respectively. The red bar marks the identical seed sequence of the families sf-miR-208a(2) and sf-miR-499(1).

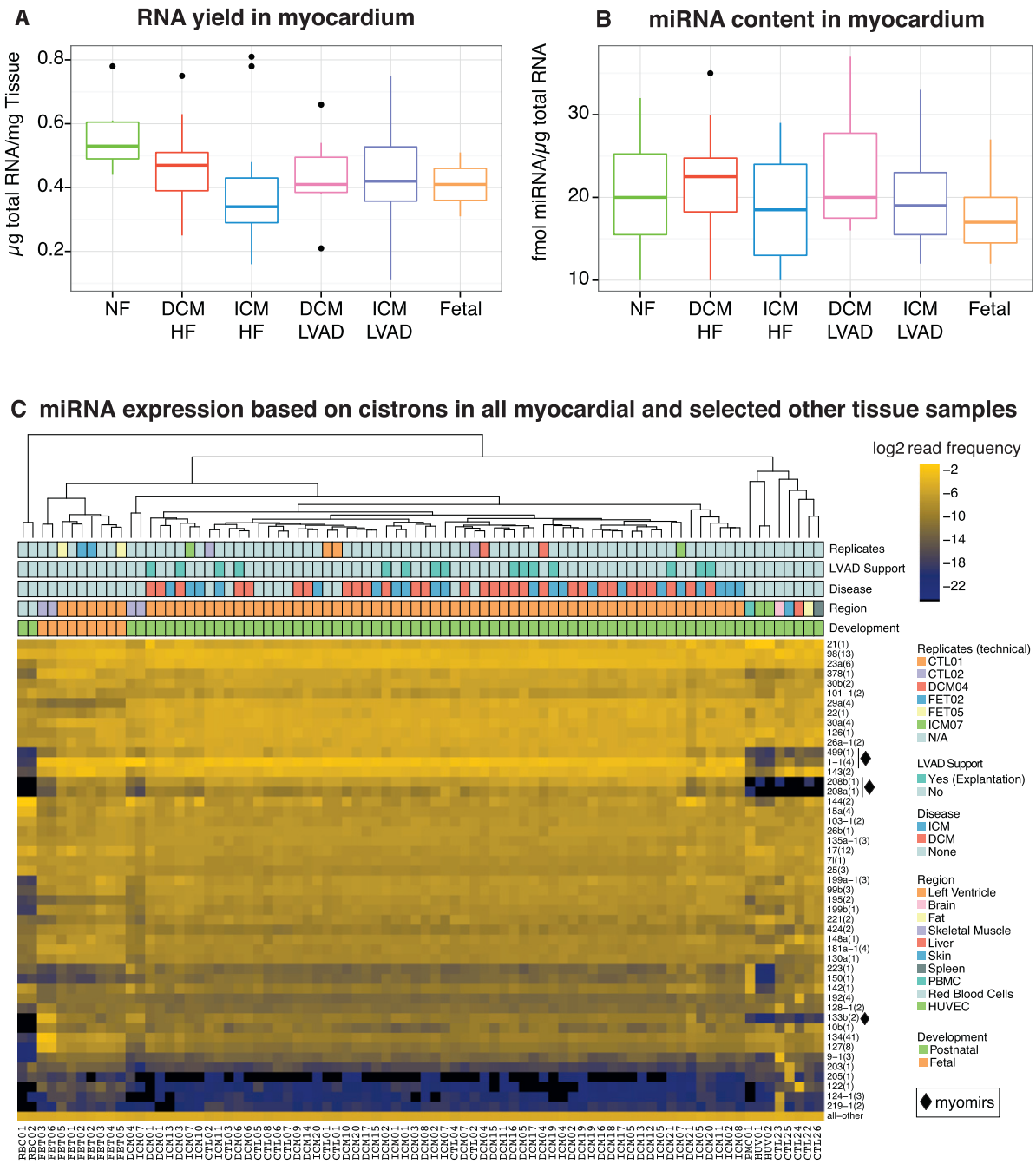

Fig. S2. RNA quantification and miRNA expression based on cistrons in all myocardial samples. (*A* and *B*) RNA yield (*A*) and miRNA content (*B*) in myocardial samples for the individual groups indicated. The upper and lower hinges of the box plots correspond to the 75th and 25th percentiles, respectively. The upper and the lower whiskers (lines) include values from the upper and lower hinges to 1.5 * the interquartile range; the dots represent outliers beyond these values. (*C*) Unsupervised clustering of miRNA cistrons contributing to the cumulative top 85% sequence reads of all solid tissue and primary cell samples included in this study; the rows were labeled with unique cistron numbers omitting the "mir-" prefix. There is a clear separation between fetal and postnatal tissue, striated muscle tissue, and nonmuscle tissue, as well as a clear separation between the two striated muscle tissues, namely skeletal and cardiac muscle. However, differences between the nonfailing and failing myocardial samples are too low to separate healthy and diseased samples. The topmost annotation track marks technical replicates revealing a small intersample distance as indicated by the dendrogram leaves. The FET2 replicate was a technical replicate of the same isolated RNA in one sRNA cDNA library preparation, and the CTL01 replicate was from different RNA isolations from the same tissue sample used in one sRNA cDNA library preparation; the very small distance between these replicates highlights the low technical variance of the sRNAseq protocol. All other technical replicates were prepared in different experiments, using in part different RNA isolations. Note that even in these cases there are no noticeable differences in the profiles.

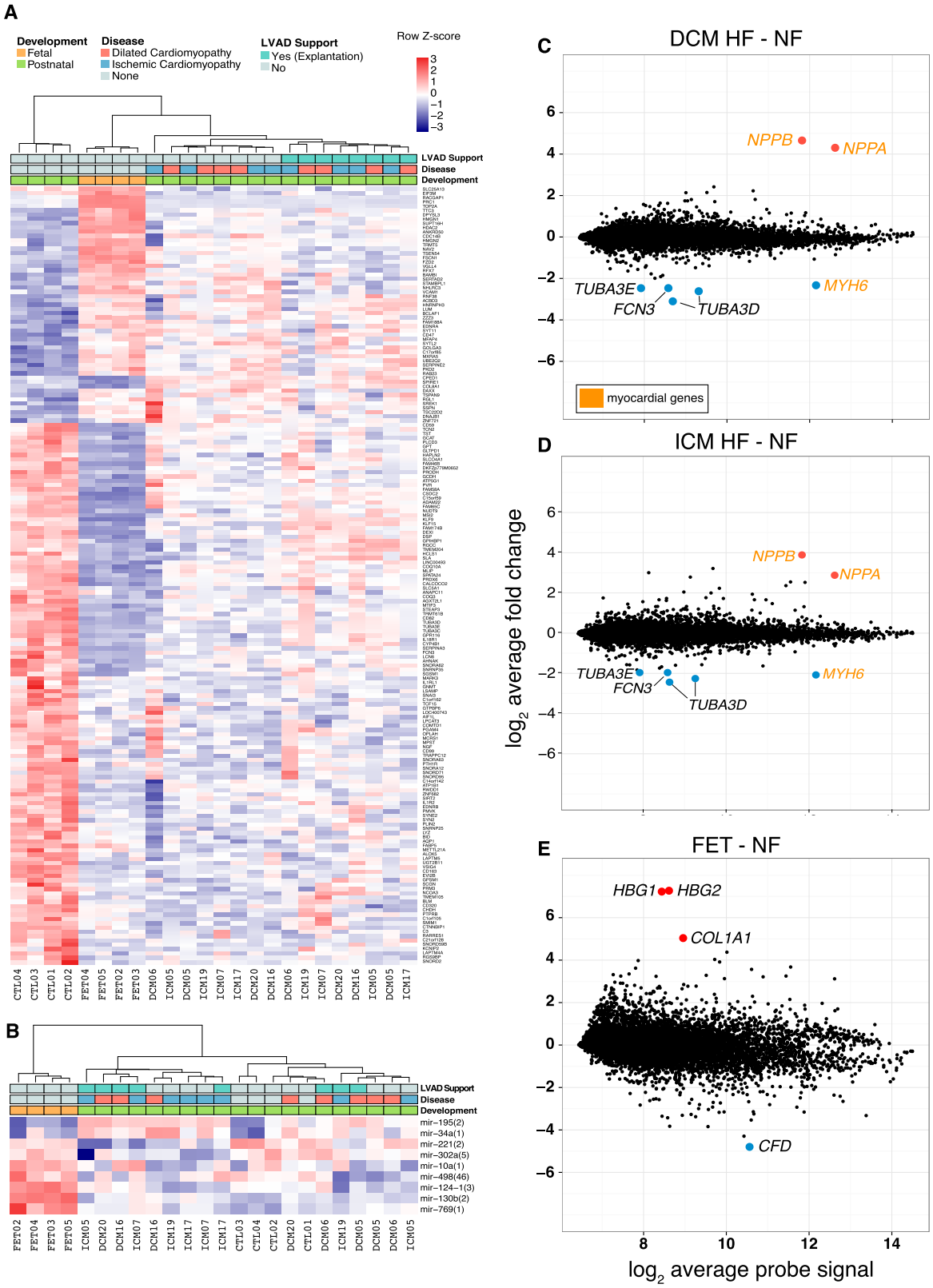

Fig S3. Gene expression profiles in fetal and failing myocardium. (*A* and *B*) Hierarchical clustering of the intersection of mRNAs (*A*) and miRNA cistrons (*B*) differentially expressed in DCM or ICM HF myocardium (i.e., at LVAD implantation) and in fetal hearts (FETs) compared with nonfailing postnatal myocardium (NFs) at an FDR of 5%. Rows and columns were clustered using Euclidean distance and Ward's method clustering; the row dendrograms were removed. (*C*–*E*) MA plots for the comparisons indicated in the plot titles. The breaks and limits on the *y* axes correspond to those in Fig. 2 *A* and *B* to facilitate the comparison. The genes with the biggest absolute differences are labeled as are some genes related to HF (*NPPA* and *NPPB*) and/or myocardial function (*MYH6*): they are labeled red if up-regulated or blue if down-regulated (FDR < 10%). Note that not all genes with an FDR < 10% were color-coded. Details oM the mRNA expression changes for all genes with an FDR < 10% can be found in Dataset S1 (Tables 17 and 18).

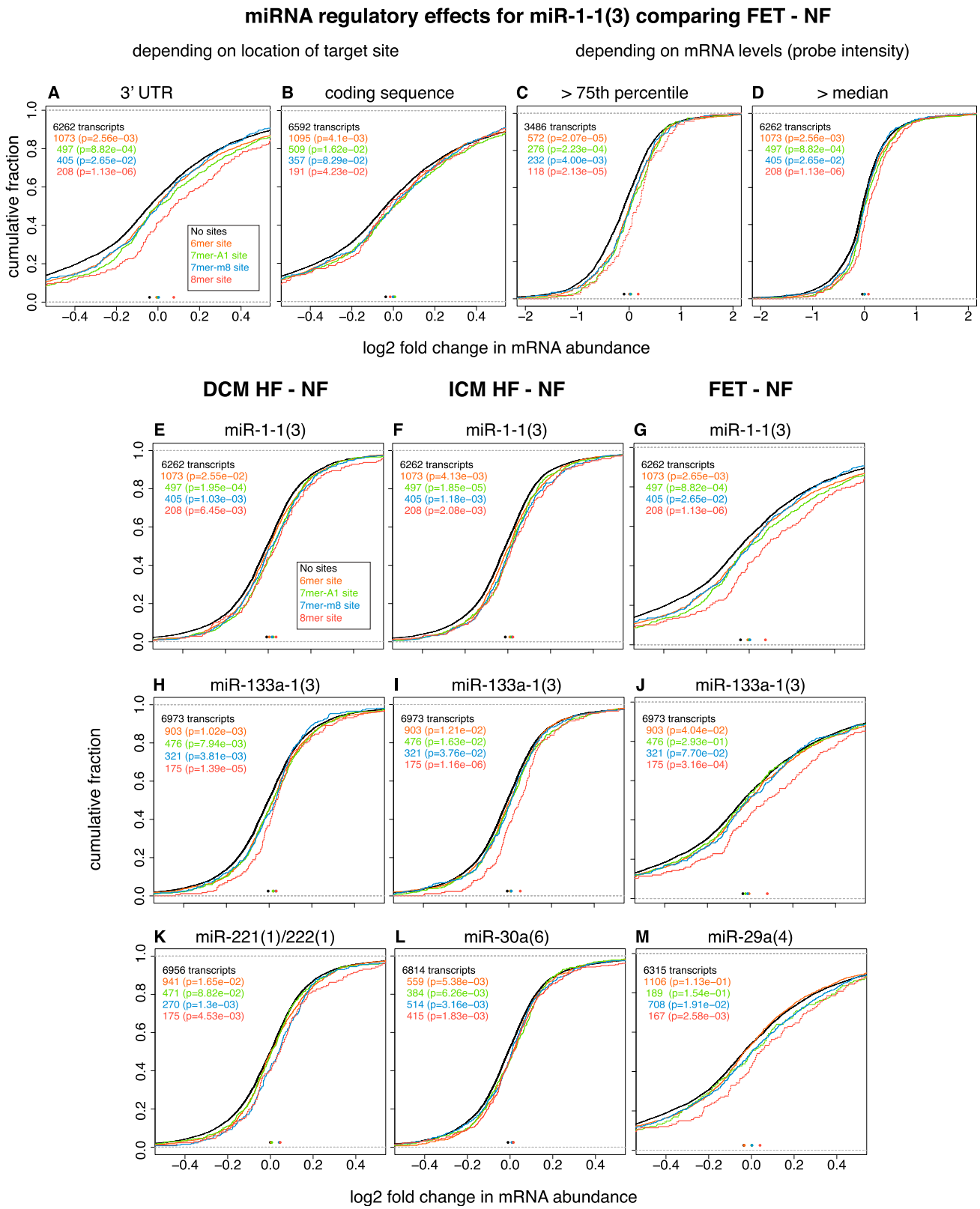

Fig. S4. miRNA regulation for abundant and changed miRNAs. (*A–D*) mRNA expression changes in FETs compared with NFs for sf-miR-1-1(3). This miRNA family comprising miRNAs miR-1(2) from cistrons mir-1-1(4) and miR-206 from cistron mir-133b(2) was threefold lower in FET than in NF [Dataset S1 (Table 3)]. (*A* and *B*) Differences on miRNA regulation based on the location of the miRNA seed site in the (*A*) 3′-UTR or (*B*) coding sequence, and (*C* and *D*) depending on mRNA abundance as determined with Illumina HumanHT-12 v4 BeadChips selecting the (*C*) 75th percentile and the (*D*) median probe intensities as cutoff. (*E–M*) Changes in mRNA abundance in a seed-type-dependent manner for mRNA targets with miRNA target sites in the 3′-UTR for the families miR-1-1(3) (*E–G*), miR-133a-1(3) (*H–J*), and selected other miRNAs (*K–M*), comparing myocardium from patients with dilated cardiomyopathy at LVAD implantation (DCM HF)

Legend continued on following page

(*E*, *H*, and *K*), from patients with ischemic cardiomyopathy at LVAD implantation (ICM HF) (*F*, *I*, and *L*), and FETs (*G*, *J*, and *M*) to NFs. All shown miRNA families were down-regulated/lower in the DCM/ICM HF or FET compared with NF. Note: Families miR-221(1) and miR-222(1) have the same seed sequence (5′-nucleotides 1–8; Dataset S1 (Table 38)], but are grouped into different sf due to differences in the remaining mature sequences. Color-matched dots at the bottom represent the median of each cumulative distribution function.

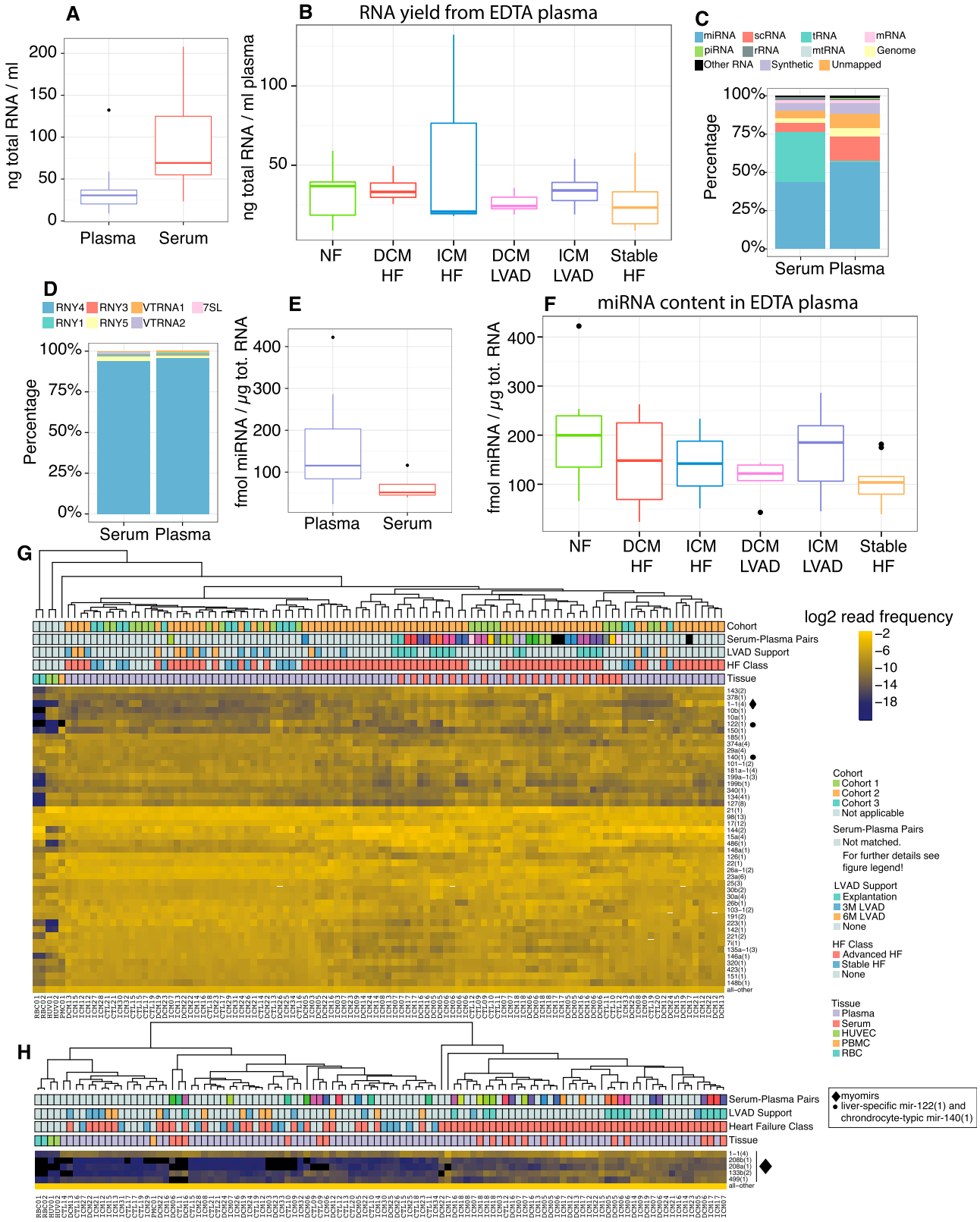

Fig. S5. RNA quantification and circulating miRNA composition based on cistrons in all serum and plasma samples used in this study. RNA yields from (*A*) plasma ($n = 85$) and serum ($n = 18$) and from (*B*) plasma samples for the individual clinical conditions as indicated. (*C*) Differences in RNA composition between serum ($n = 18$) and plasma ($n = 85$) samples by sRNAseq. The "Synthetic" category summarizes reads from spiked-in calibrators, adapters, size markers, and reads associated with recombinant protein production [see Dataset S1 (Table 36) for details]. (*D*) Detailed distribution of the scRNA RNA fraction in serum ($n = 18$) and plasma ($n = 85$) samples. The Y RNA RNY4 contributes to the vast majority of sequenced fragments. A reported transcript called RNY2 was falsely annotated as Y RNA and therefore was not included here. Different sequence variants of the Y RNAs (RNY1 and RNY3–5), vaultRNAs (vtRNAs), and 7SL

Legend continued on following page

fractions have been omitted due to their low contribution. (*E* and *F*) Differences in miRNA content per microgram of total RNA (*E*) between plasma and serum and (*F*) between plasma samples of the different clinical groups investigated. (*G*) Unsupervised hierarchical clustering of all plasma and paired serum samples, where available, together with hematopoetic and endothelial cells. Paired serum and plasma samples (i.e., collected from the same patient at the same time) are indicated by identical colors in the corresponding annotation track above the heatmap. Using the most abundant miRNAs, i.e., miRNAs contributing to the top 85% sequence reads, there is basically no difference between serum and plasma samples; it should be noted, however, that the plasma samples were not platelet depleted. The serum–plasma pairs were prepared during the same experiment but in separate sRNA cDNA libraries. Furthermore, the different HF classes do not separate. Myomir mir-1-1(4) (diamond), the liver-specific mir-122(1), and the chondrocyte-typic mir-140(1) are the only tissue-enriched miRNAs other than hematopoetic or endothelial miRNAs detected in the majority of sequence reads. All other miRNAs are either specific to hematopoetic/lymphatic or endothelial cells or ubiquitously expressed. (*H*) Unsupervised hierarchical clustering of only the myomir cistrons of the same samples as in *G*. Due to the strong increase in the circulating myomir concentration, the advanced HF samples before LVAD support (i.e., at implantation) or at LVAD explantation clearly separate from (*i*) patient-matched advanced HF samples 3 or 6 mo after the initiation of LVAD support, (*ii*) from patients with stable HF, and (*iii*) healthy controls. Some of the serum–plasma pairs cluster with bigger differences than in *G* because of the higher variability in the low abundant myomirs in circulation. The upper and lower hinges correspond to the 75th and 25th percentiles, respectively. The upper and the lower whiskers (lines) include values from the upper and lower hinges to 1.5 * the interquartile range; the dots represent outliers beyond these values.

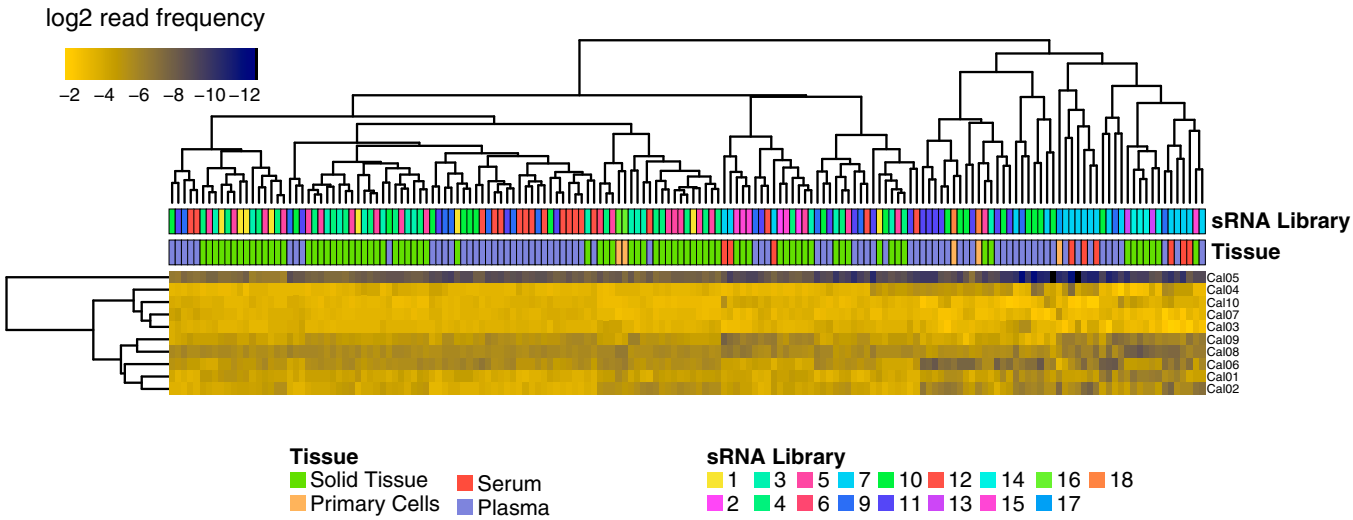

Fig. S6. Unsupervised hierarchical clustering of external RNA standards. Ten synthetic 22-nt external reference oligoribonucleotides (calibrators) were added in equimolar amounts to the sample RNA during the sRNA cDNA preparation. These calibrators can be used for miRNA quantification and library quality control. The calibrators were designed to reflect the different ligation efficiencies of naturally occurring (small) RNAs, with calibrators like Cal05 or Cal08 being less efficiently carried through the library preparation than others. The calibrator reads for all 14 libraries that were supplemented with external reference RNA were converted to the log2 read frequencies and subjected to agglomerative hierarchical clustering using Euclidean distance metrics and the complete linkage algorithm for column and row clustering. Please note that library 8 (serum and plasma samples) was not spiked-in with external standards and as such is not shown here.

Table S1. Demographics and clinical data on left ventricular tissue donors

Characteristic	NF $n = 8$	DCM HF $n = 21$	ICM HF $n = 13$	FET $n = 5$
Age, median (range)*	48 (2–80)	57 (33–78)	66 (51–78)	21 (19–23)
Sex: male %	63	95	92	Unknown
Race (%)				
Caucasian	4 (50)	14	11	0
African American	0 (0)	5	0	1
Asian	1 (12.5)	0	1	0
Hispanic	0 (0)	2	0	0
Unknown	3 (37.5)	0	0	4
LVEF, median (range)†	57/65 (6 unknown)	15 (10–30)	17.5 (10–22)	Unknown
Comorbidities (%)				
Hypertension		9 (43)	7 (54)	
Diabetes		10 (48)	2 (15)	
Lipid disorders		5 (24)	8 (62)‡	
Medication (%)				
Acetylsalicylic acid		6 (29)	9 (69)‡	
β-Blockers		17 (81)	11 (85)	
RAAS Inhibitors		14 (67)	3 (23)‡	
Statins		6 (29)	8 (62)	
Laboratory values				
Alanine aminotransferase, U/L		21 ± 11	26 ± 18	
Aspartate aminotransferase, U/L		21 ± 8	38 ± 29‡	
Total bilirubin, mg/dL		1.3 ± 1.1	2.4 ± 2.3	
Creatinine, mg/dL		1.5 ± 0.4	1.6 ± 0.5	
Hemoglobin, g/dL		15 ± 10	14 ± 10	
Platelet count, $10^3/\mu L$		207 ± 59	161 ± 47‡	

RAAS, renin-angiotensin-aldosterone system.

*For fetal samples age in weeks.

†Left ventricular ejection fraction (LVEF) known for two controls at the time of tissue procurement.

‡$P < 0.05$ between advanced HF with DCM and ICM.

Table S2. Demographics and clinical data on serum and plasma donors

Characteristic	NF $n = 13$	Stable HF $n = 14$	Advanced HF $n = 24$
Age, median (range)*	60 (32–70)	63 (49–71)	66 (33–78)
Sex: male %	69	79	92
Race (%)			
Caucasian	8 (62)	7 (50)	18 (75)
African American	2 (15)	3 (21)	3 (13)
Asian	0 (0)	0 (0)	0 (0)
Hispanic	3 (23)	1 (7)	0 (0)[†]
Unknown	0 (0)	3 (21)	3 (13)
LVEF, median (range)	Unknown	22 (10–43)[‡]	18 (10–24)
NYHA		3.1 (2–4)	3.5 (2.5–4)
Comorbidities (%)			
Hypertension	0	11 (79)	11 (46)
Diabetes mellitus	0	5 (36)	10 (42)
Hyperlipidemia	0	10 (71)	11 (46)
Medication (%)			
Acetylsalicylic acid		11 (79)	12 (50)
β-Blockers		11 (79)	20 (83)
RAAS Inhibitors		10 (71)	14 (58)
Statins		11 (79)	14 (58)
Laboratory values			
Alanine aminotransferase, U/L		22 ± 9	26 ± 19
Aspartate aminotransferase, U/L		23 ± 11	31 ± 24
Total bilirubin, mg/dL		1.0 ± 0.6	1.6 ± 1.8
Creatinine, mg/dL		1.6 ± 1.6	1.4 ± 0.5
Hemoglobin, g/dL		13 ± 2	15 ± 9
Platelet count, $10^3/\mu L$		193 ± 37	197 ± 76

*For fetal samples age in weeks.
[†]$P < 0.05$ between advanced HF and NFs.
[‡]$P < 0.05$ between advanced and stable HF.

Other Supporting Information Files

Dataset S1 (XLS)